Characterization and Comparison of Piezoresistive Materials and Their Performance on Pressure-Sensitive Mats

Javier Martínez-Cesteros, Sergio Domínguez-Gimeno, Julián Castellanos-Ramos, José A. Sánchez-Durán, and Carlos Medrano-Sánchez

***Abstract*—The response of three readily available low-cost piezoresistive materials (EeonTex, Ex-Static, and Velostat) and their performance on a specific application were studied in this work. First, a series of pressure cycles was applied with a pneumatic platform on piezoresistive sensors based on them. These experiments allowed quantifying several nonidealities: Variability, drift, creep, hysteresis, nonlinearity, and response time. An overview radar chart showed that hysteresis, variability, and response time were quantitatively more relevant and different between the materials. Then, pressure-sensitive mats (PSMs) were manufactured using each of those three materials. They were evaluated by measuring the center of pressure (CoP) in stability tests. A force platform (FP) served as a reference instrument. The best performance in this kind of experiment was obtained by the Velostat-based mat (trajectory distance of 0.021 versus 0.035 and 0.045 cm/sample for Ex-Static-based and EeonTex-based mats, respectively). This material also showed less response time (0.21 versus 0.42 and 0.50 s for Ex-Static and EeonTex, respectively) and hysteresis (0.11 versus 0.21 and 0.23 S/S for EeonTex and Ex-Static, respectively), although its variability was larger (0.137 versus 0.065 and 0.059 S/S for Ex-Static and EeonTex, respectively). These results indicate that response time and hysteresis have a major influence on the determination of the CoP. Further research should focus on compensating for these effects or finding sensor configurations that minimize them.**

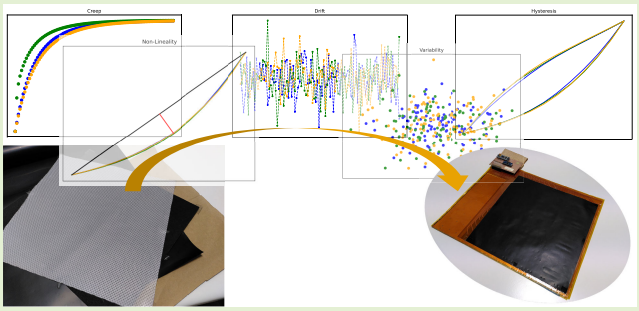

***Index Terms*—Center of pressure (CoP), creep, drift, EeonTex, Ex-Static, force platform (FP), hysteresis, linearity, piezoresistive sensor, resistive sensor array, stability test, tactile sensor, variability, velostat.**

Received 9 July 2025; revised 8 September 2025; accepted 21 September 2025. Date of publication 1 October 2025; date of current version 14 November 2025. This work was supported in part by "Departamento de Ciencia, Universidad y Sociedad del Conocimiento, del Gobierno de Aragón" under Grant T49_23R; in part by MICIU/AEI/10.13039/501100011033/ and FONDO EUROPEO DE DESARROLLO REGIONAL (FEDER), UNIÓN EUROPEA (UE), under Grant PID2021-125091OB-I00, Grant PID2024-158986OB-C21, and Grant PID2024-158986OB-C22; and in part by Plan de Recuperación, Transformación y Resiliencia (Unión Europea-Next Generation), Proyecto Estratégico del Instituto Nacional de Ciberseguridad (Spain) under C077/23. The work of Sergio Domínguez-Gimeno was supported by Spanish "Ministerio de Ciencia, Innovación y Universidades" under Grant FPU-20/04578. The associate editor coordinating the review of this article and approving it for publication was Dr. Nirupama Mandal. *(Corresponding author: Javier Martínez-Cesteros.)*

This work involved human subjects in its research. Approval of all ethical and experimental procedures and protocols was granted by Comité de Ética de la Investigación de la Comunidad Autónoma de Aragón (CEICA) (Reference: 22/2019 and Protocol Version: 1.0, 29-11-2019).

Javier Martínez-Cesteros, Sergio Domínguez-Gimeno, and Carlos Medrano-Sánchez are with EduQTech, E.U. Politécnica, 44003 Teruel, Spain, and also with the University of Zaragoza, 50009 Zaragoza, Spain (e-mail: javimzcs@unizar.es; sdominguezg@unizar.es; ctmedra@unizar.es).

Julián Castellanos-Ramos and José A. Sánchez-Durán are with Departamento de Electrónica, Universidad de Málaga, 29071 Málaga, Spain, also with the Instituto de Investigación Biomédica de Málaga, 29590 Málaga, Spain, and also with the Instituto Universitario de Investigación en Ingeniería Mecatrónica y Sistemas Ciberfísicos (I3MSC), 29071 Málaga, Spain (e-mail: jcramos@uma.es; jsd@uma.es).

Digital Object Identifier 10.1109/JSEN.2025.3614471

I. Introduction

PRESSURE transducers are sensors capable of measuring the force applied to their surface from the change in an electrical quantity. There are several types of pressure-sensitive sensors [1], [2]. In the so-called contact pressure sensors the pressure exerted is applied by directly touching the sensor. These sensors have several applications, such as providing touch to robotic manipulators [3], measuring the buccal pressure exerted by the tongue [4], monitoring the pressure exerted while sleeping [5], or monitoring heart rate [6] among many others [7].

However, complex nonlinear sensor responses greatly influence their performance in practical applications. Sánchez-Durán et al. [8] showed how pressure images are different in a 16×16 tactile sensor for increasing and decreasing applied pressures, and how these differences are minimized if hysteresis is compensated. Lee et al. [9] developed a skin mountable stretch sensor to measure the rotation angle of the wrist. They found that compensating for hysteresis allowed decreasing the angle error of the device. A polynomial model showed 5.43° error, while a model that took hysteresis into account only showed 1.93° error in static measurements in the range about 10°–70°. Arndt [10] used an insole with capacitive sensors for long-term (3 h) plantar pressure monitoring. An increase in sensor response of up to 17% for that period was found.

This should be corrected for reliable pressure determination. Chacko and Sivakumar [11] also reported the effect of creep in a foam rubber optical pressure measurement system. In an experiment of 8 min, the error of models that do not take creep into account was up to 10%. Han et al. [12] designed and tested a soft ground reaction force sensor integrated into an insole for gait analysis. The sensor exhibited nonlinear response and hysteresis. The compensation of hysteresis using a recurrent neural network decreased the error by 64%. Park et al. [13] also acknowledged the importance of nonlinear and hysteretic behavior. They developed a novel wearable sensing brace design for measuring multiple degrees of freedom ankle motions. The design minimized hysteresis and improved the measurement repeatability.

Although there is ongoing research to produce reliable sensors with high sensitivity and sensing range, which can be integrated into wearable devices [7], [14], this article deals with low-cost systems that can be manufactured with standard, simple, and fast procedures. They are based on off-the-shelf piezoresistive materials. Their typical structure consists of two electrodes and a piezoresistive sheet that interconnects them, but other configurations are possible. They are sensitive mainly to perpendicular force, although there are structures that allow 3-D sensitivity [15]. Unfortunately, the response of these sensors is far from an ideal behavior, presenting a series of limitations [16], [17], [18]. This work analyzes some of these drawbacks, which are listed in Section I-A.

A. Nonidealities Description

The following typical nonidealities of pressure sensors have been analysed.

1) Variability: The difference between the sensor response under several applications of the same pressure value at different times.

2) Drift: It is the effect of fluctuations over short time periods under a constant value of pressure, following the notation of [19]. This phenomenon is linked to stochastic noise in the measurement.

3) Creep: Trend in the measurement over a long time period under constant pressure. Sensors affected by creep do not stabilize their output around a constant value [19], [20], [21].

4) Hysteresis: The difference between sensor response for a given applied pressure depends on the previous evolution of pressure (memory effect). Hysteresis typically shows up in hysteresis loops in which the sensor response versus pressure follows different paths for increasing and decreasing applied pressures [22].

5) Nonlinearity: Difference between the measured values for a given pressure range and the best linear fit to them [23], [24], [25].

6) Response Time: Piezoresistive sensors cannot follow the changes of pressure instantaneously. Response time is relevant for many applications that involve dynamic measurements [14].

B. Application: Human Stability Tests

One of the applications of piezoresistive sensors is the measurement of pressure distributions, which in turn are useful in the determination of human stability [26], [27], [28]. For that purpose, sensitive units are arranged in a matrix over a large area. This type of configuration is commonly referred to as pressure-sensitive mat (PSM). The main outcome in balance studies is the center of pressure (CoP) and a recent study considers the optimal design of a PSM for CoP measurements [29]. The reference instrument to quantify it is the force platform (FP), although they are bulky and expensive devices.

C. Objectives and Contributions

The objective of the article is to make a comparison of three low-cost piezoresistive materials, both in their response to pressure in a controlled environment and in their ability to measure variations of CoP in stability tests.

The novelty of this article is twofold. First, a very complete characterization of three low-cost materials has been carried out using six parameters related to their nonideal behavior. Table I compares this work with similar previous studies that characterize piezoresistive sensors and shows that no previous study has considered so many effects and so many materials at the same time. Second, our study is the first one that describes the differences in PSMs based on different materials to quantify the CoP and their relation to the nonideal behavior measured in a controlled environment. None of the studies in Table I proposed this kind of dual performance evaluation in two different contexts. This work is partially based on the doctoral dissertation of Martínez-Cesteros [30]. The article extends it in the following aspects: 1) the way in which nonideal behavior of materials is quantified has been improved; 2) response time and nonlinearity have been included as nonidealities; 3) PSMs with up to three materials have been tested to measure CoP; and 4) more volunteers have been included to better support conclusions about CoP measurements.

D. Paper Structure

The remaining of this article is structured as follows. Section II describes the structure of the sensors as well as the instruments used to characterize their response. The sequences of pressures applied in a pneumatic chamber and the parameters obtained from these tests are explained in detail. The stability tests and the volunteer data are also described. The results obtained in the characterization tests for nonidealities are presented in Section III, while the performances for measuring CoP are presented in Section IV. Finally, the main conclusions are outlined in Section V.

II. Materials and Methods

A. Description of Sensor Arrays

All the arrays were built with the same principle: electrodes were manufactured on a regular printed circuit board (PCB) and the piezoresistive material was placed over it. The low-cost materials selected are commercially available, which allows easy prototyping of pressure sensors. Velostat

TABLE I
COMPARISON WITH PREVIOUS STUDIES

Article	Applied Force (N)	Taxel Dimensions (mm)	Material	Measured Effects
Barba-2015 [31]	0-39.24	70x145 30x68 5x5	Velostat	Repeatability Replicability Sensitivity
Dzedzickis-2020 [32]	0-3	5x5	Velostat	Roughness Sensitivity Hysteresis Transverse resolution Response time Compression deformation
Ferreira-2018 [33]	2-210	7.5x7.5	Eontex-yarns Eontex-Satanex Velostat-Satanex	Repeatability Sensitivity Speed response
This work	0-69.31	⌀10	Velostat Eontex Ex-Static	Variability Drift Creep Hysteresis Linearity Response time

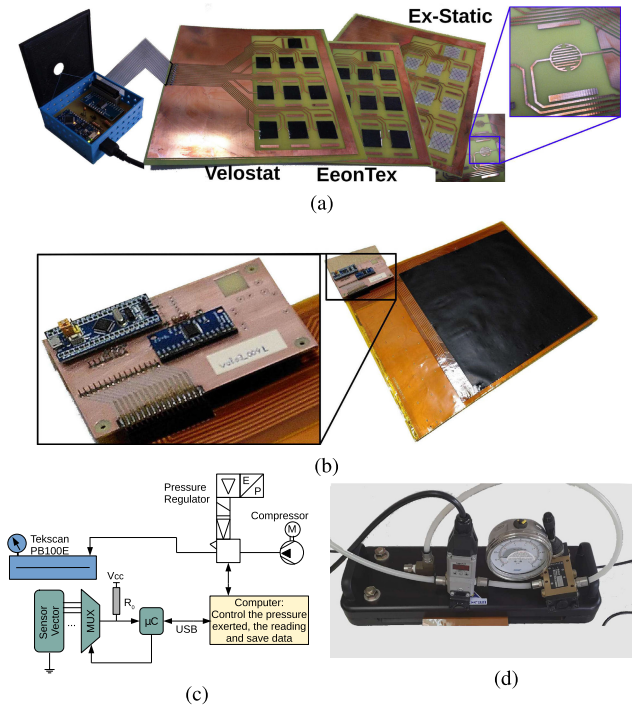

Fig. 1. Measurement systems employed. (a) Characterization arrays of the three materials with DAQ and an inset of the electrodes. (b) PSM with an inset of the DAQ. (c) Block diagram of the pneumatic pressure measurement system. (d) Pneumatic pressure system.

is a carbon-impregnated polyolefin foil (surface resistivity <31 kΩ/sq, thickness 0.1 mm). EeonTex is a nonwoven microfiber 70% polyester-30% nylon carbon-impregnated (surface resistivity 200 Ω/sq, thickness 0.8 mm). Finally, Ex-Static is a 87% polyester with 13% gray BASF Resistat (carbon) fibers woven right into the fabric (surface resistivity 10^5 Ω/sq, thickness 0.05 mm). Two different types of sensor arrays were built for each material. One of them is a small-sized array that fits in a pneumatic platform. This type of array was used for sensor characterization. The other array is larger, about the size of a mat. It allows obtaining pressure images of a person's feet in balance tests.

1) Description of the Array for Characterization: Three PCB were manufactured, one for each material: Velostat, EeonTex, and Ex-Static. A taxel is made of interdigital electrodes, circular in shape, 10-mm diameter, over which a piece of piezoresistive material is attached manually with adhesive tape, Fig. 1(a). Each printed circuit board (PCB) has ten taxels, so that ten conductances were obtained for a given test. It is worth pointing out that the parameters listed in Section II-B were calculated for each taxel separately, but the results in Section III refer to their average values for the sake of simplicity. Nevertheless, confidence intervals of the mean have been included in the figures.

Each taxel has two independent electrical connections and a ribbon cable transmits the signals between the data acquisition system (DAQ) and the PCB, Fig. 1(a). The DAQ is responsible for selecting each taxel sequentially by means of an analog multiplexer. The two electrodes of a taxel are connected to ground and to a 2.2-kΩ resistor, respectively. The resistor is powered by 5 V. The output of this voltage divider is connected to a 10-bit analog to digital converter (ADC) of a microcontroller (μC) (Arduino nano every). The input resistance of the ADC is close to ideal, while the multiplexer has an internal resistance of 57 Ω. The sampling frequency is 2 Hz, except for transient response characterization, in which 16 Hz is set in order to measure response times below 1 s. An additional thermistor is included in the DAQ system as another input of the analog multiplexer. It allows measuring temperature during the experiment.

2) Description of the PSMs: Our PSM, Fig. 1(b), is a 16 × 16 array of taxels covering a surface of 32 × 32 cm. The electrode shape is the same as in the array for characterization (interdigital, circular in shape, 10-mm diameter). The base layer is a flexible PCB. PSMs are available with the piezoresistive materials to be tested: Velostat, EeonTex, and Ex-Static. A sheet of material covers the entire surface of the electrodes. It is manually placed on top of the PCB and fixed with adhesive tape, Fig. 1(b).

In this case, the electrodes share row and column connections. The DAQ selects each row and column of the PSM, connecting them to ground and to a 2.2-kΩ resistor powered by 3.3 V. This voltage divider is connected to a 12-bit ADC of a STM32F103C8T6 μC. The μC sends data to a PC via USB. A complete scanning of the mat is performed at 100 Hz. The internal resistance of the multiplexers is 157.6 Ω, while the input resistance of the ADC can be considered as ideal. More details about the DAQ circuit are available in [34]. However, a crosstalk effect between taxels appears if there are common row and column connections. This effect is clearly observed in pressure images since there seems to be pressure exerted on some regions even if there is no object on it. This is why it is sometimes referred to as ghost effect. We have corrected it using the algorithm described in [34]: It has been shown that the quantity obtained when a row-column pair is selected is the equivalent resistance between that pair, not the taxel resistance. After a scan of the whole array, the taxels resistances can

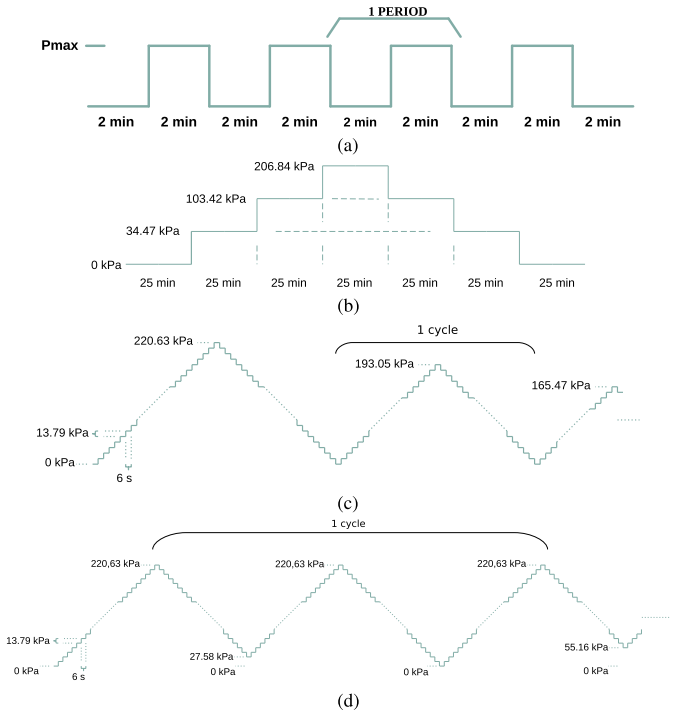

Fig. 2. Representations of the pressure applied in the pneumatic test. (a) Rapid cyclic test. (b) Long duration test. (c) Descendent hysteresis test. (d) Ascendant hysteresis test.

be calculated from the set of equivalent resistances. Finally, CoP is calculated in PSMs by applying a proportional relation between conductance and pressure. Crosstalk elimination is a prerequisite before analyzing pressure images. Otherwise, their quality is very bad, showing rectangular in shape objects and a clear worse CoP measurement (see [34, Fig. 12] or [35, Fig. 5]).

B. Tests With a Pneumatic Platform

The pneumatic system is made of an equilibration device PB100E from Tekscan [36] controlled by a proportional pressure regulator 171E2N.T.D.0009 from Pneumax [37], see Fig. 1(c) and (d). The system is managed by a LabView[1] program that allows regulating the pressure and capturing data from a PC. The regulator operates with the imperial measurement system (psi).

This pneumatic system is a suitable device to apply a uniform and regulated pressure over the small-sized arrays for characterization. Four types of tests have been performed.

The first test (rapid cyclic test) involved applying 20 periods of loading (120 s) and unloading (120 s) with a constant load value ($P_{\max}$). This test was repeated for two values of $P_{\max}$, 34.47 kPa (5 psi) and 103.42 kPa (15 psi), with a resting time of 80 min between them. The goal of this test is to characterize variability. It is shown schematically in Fig. 2(a).

The second test (long duration test) involved applying a constant pressure level for 25 min and then change it to another pressure level. The levels were applied first in ascending order and then in descending order: 0 kPa, 34.47 kPa (5 psi), 103.42 kPa (15 psi), and 206.84 kPa (30 psi). This test was used for drift and creep characterization, and it is shown in Fig. 2(b). The constant load periods are longer than in the previous test, but at the same time not too long in order to ensure that the pneumatic platform can maintain a constant pressure level.

The third test (hysteresis) was further subdivided into two tests. In the first one, loading-unloading cycles were applied in which the maximum pressure value was decreased each time (descendent cycles). In the second one, loading-unloading cycles were applied in which the point to rise from was increased each time (ascendant cycles) [8], [38]. Pressure changed every 6 s in 13.79 kPa (2 psi) steps, and maximum and minimum values were multiples of 27.58 kPa (4 psi). In the descendent cycles the limiting pressure values were (in kPa): 0, 220.63; 0, 193.05; 0, 165.47; 0, 137.90; 0, 110.32; 0, 82.74; 0, 55.16; 0, 27.58; 0. In the ascendant cycles those values were (in kPa): 0, 220.63, 27.58, 220.63; 0, 220.63, 55.16, 220.63; 0, 220.63, 82.74, 220.63; 0, 220.63, 110.32, 220.63; 0, 220.63, 137.90, 220.63; 0, 220.63, 165.47, 220.63; 0, 220.63, 193.05, 220.63; 0.

This test is better understood graphically as in Fig. 2(c) and (d) in which the sequence of pressures is presented. The whole set of cycles was repeated ten times, and the results were averaged.

The fourth test was devoted to determine response time just after a step in pressure. In this case, it is more important to get a change as abrupt as possible. Thus, the pneumatic platform was configured to apply a pressure of 103.42 kPa (15 psi) and hold it for 6 s, but no further regulation was performed to correct the pressure if the final set point was not exactly reached. This experiment aims to characterize short-term response (below 1 s), which can be relevant for the detection of human movements for instance. Therefore, the sampling frequency was changed to 16 Hz in this experiment. This complements the second test that targets long-term behavior.

From the tests explained above, the nonideal behavior described in Section I-A can be quantified.

1) *Variability:*
For each period in Fig. 2(a), the average of the conductance in the last 30 s is calculated. In this way, a value per period is obtained, g_{period}. A measure of variability is the coefficient of variation (CV) [19], [39], defined as the ratio of standard deviation ($\sigma_{g_{\text{period}}}$) over the mean value ($\overline{g}_{\text{period}}$)

$$\text{Variability} = \text{CV} = \frac{\sigma_{g_{\text{period}}}}{\overline{g}_{\text{period}}}. \tag{1}$$

2) *Drift:*
To quantify drift, the sensor response after a change in pressure, Fig. 2(b), is divided into nonoverlapping 30-s windows. This windowing reduces the effect of other nonidealities, in particular creep. Besides, only the second half of the response, 12.5 min, is processed to avoid other possible effects just after the abrupt change in pressure. In this way, 25 windows for each pressure level are obtained. For each window, the

[1] Trademarked.

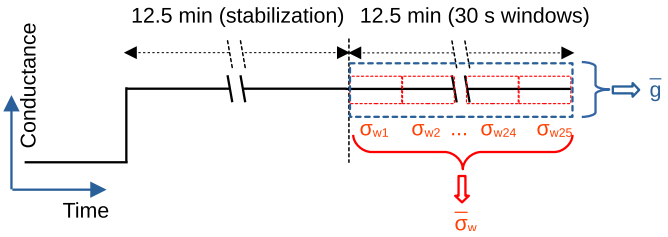

Fig. 3. Schematic view of the drift quantification. After a change in pressure level, 12.5 min are left out for stabilization of conductance. The remaining 12.5 min are divided into 25 windows of 30 s. In each window the standard deviation, σ_{wi}, is obtained, and then its average, $\overline{\sigma_w}$. Then, this average standard deviation is divided by the mean conductance of the last 12.5 min, $\bar{g}$.

standard deviation of the conductance is calculated, σ_{wi} ($i = 1, \ldots, 25$). Finally, a parameter to characterize the drift is the average of those values for all the windows, normalized by the mean value of the signal in the periods considered ($\bar{g}$) [19]

$$\text{Drift} = \frac{\overline{\sigma_w}}{\bar{g}}. \tag{2}$$

Fig. 3 shows schematically the drift calculation based on a 25-min period of constant load application.

3) *Creep:*
To quantify Creep we follow [19] using the long duration test. For each value of applied pressure, the slope of the conductance, slope(g), is calculated in the second half of the loading time to discard transient effects. The creep parameter is the absolute value of the slope normalized by the mean conductance, $\bar{g}$, in the period considered

$$\text{Creep} = \frac{|\text{slope}\,(g)|}{\bar{g}}. \tag{3}$$

4) *Hysteresis:*
To quantify hysteresis the difference between the conductance when the pressure is first increased (g_{up}) and then decreased (g_{down}) is taken into account as in [38] and [40]. The maximum value of their difference, $\max(|g_{\text{up}} - g_{\text{down}}|)$, is computed and then normalized by the conductance span of the loop, $\max(g) - \min(g)$, (4). A value is obtained for each hysteresis loop both in the descendent and ascendant series described previously in this section

$$\text{Hysteresis}\,(g) = \frac{\max\left(|g_{\text{up}} - g_{\text{down}}|\right)}{\max\,(g) - \min\,(g)}. \tag{4}$$

5) *Linearity:*
Nonlinearity is obtained from the largest hysteresis loop in the descendent test. The two conductance-pressure paths, (p_{up}, g_{up}) and (p_{down}, g_{down}), are averaged to get a single conductance versus pressure curve (p, g). Then, a linear fit is carried out and the nonlinearity is obtained from the R^2 coefficient of the fit as

$$\text{NonLin}\,(g, p) = 1 - R^2. \tag{5}$$

6) *Response Time:*
Response time is defined as the time required to reach 63% of the final conductance value after a change in pressure from 0 to 103.42 kPa (15 psi). The final conductance value is taken 6 s after the pressure step.

Fig. 4. Picture showing the configuration of the PSM and the FP in the human stability tests.

C. Stability Tests

The CoP was obtained simultaneously by an FP PS-2141 PASPORT from Pasco [41] and one of our PSM with the material under evaluation in order to compare the performance of different materials in balance tests. Data from the FP (range –1100 to 4400, and 0.1 N) and the PSM were transmitted by USB to a PC in which their respective softwares were responsible for storing them. The CoP coordinates were obtained directly from the manufacturer's software for the FP, while they were obtained from the pressure maps for the PSMs.

Each volunteer stepped onto the FP, which has on it a PSM with the material to be evaluated as shown in Fig. 4. The volunteer was asked to perform three different tests: 1) keep balance on left leg; 2) keep balance on right leg; 3) keep balance on both legs while the volunteer swayed in both medial-lateral (ML) and anterior-posterior (AP) directions, describing circles seen from above ("rotation" test for short). Each test lasted at least 30 s. They were repeated for each of the PSM with different piezoresistive materials.

Given that the platforms work independently a semi-manual technique based on cross correlation was used to synchronize their data in a post-processing step. Finally, a 30-s window from both platforms at 100 Hz was extracted for further analysis.

The average displacement in the 30-s window was substracted from the CoP coordinates. In this way, the CoP from the two devices can be compared directly and the relative position of the PSM with respect to the FP has no influence. Besides, it is worth pointing out that the absolute CoP coordinates are not important in stability studies and that the parameters extracted from them are invariant to translations. The details about the experiments and the configuration of the devices can be found in [42].

Fifteen volunteers participated in the balance tests. Their characteristics are shown in Table II. The protocol was approved by our Ethics Committee (Comité de Ética de la Investigación de la Comunidad Autónoma de Aragón, CEICA, reference: 22/2019, protocol version: 1.0, 29-11-2019).

Data associated with both tests with a pneumatic platform and tests with humans are available on gitlab.[2]

[2]https://gitlab.com/ctmedra1/piezoresistive_materials_comparison/-/releases/v202402

TABLE II
OVERALL CHARACTERISTICS OF THE VOLUNTEERS

	Mean	Std
Age (years)	28.6	10.8
Height (m)	1.71	0.07
Weight (kg)	63.8	9.1

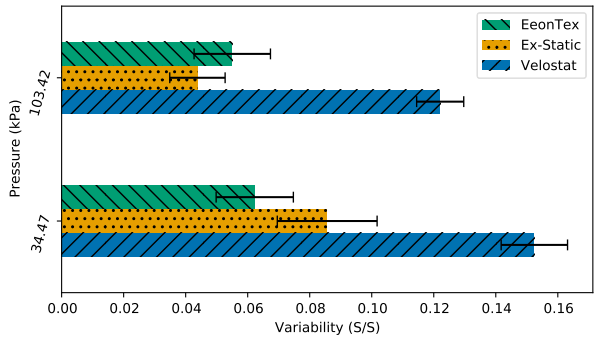

Fig. 5. Variability of the materials. Bar errors indicate confidence intervals.

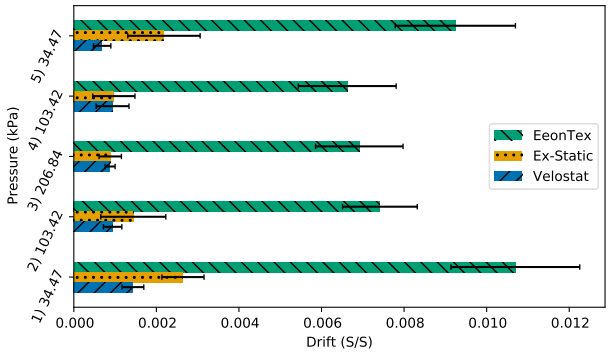

Fig. 6. Drift of the materials. On the y-axis, the ordinal number before the parenthesis indicates the order in the sequence of applied pressures. Bar errors indicate confidence intervals.

III. RESULTS OF SENSOR CHARACTERIZATION

A. Variability

The results are presented in Fig. 5. For the highest applied pressure in the rapid cyclic test ($P_{\max}$ = 103.42 kPa) Ex-Static shows less variability than EeonTex, and EeonTex shows less variability than Velostat. However, for the lowest applied pressure ($P_{\max}$ = 34.47 kPa) the EeonTex behavior is better than that of the other two materials. On average, Velostat is clearly the worst with respect to this parameter.

B. Drift and Creep

1) Drift: The results are presented in Fig. 6, separately for each value of the constant applied pressures in the long duration test. EeonTex drift is clearly above the drift of the other two materials. Taking the average values of Fig. 6, the influence of drift is lower in Velostat than in Ex-Static.

2) Creep: The creep effect can be seen in Fig. 7. Although the values seem to be low, it should be noted that the influence on a measurement increases with the load duration, so that it is more noticeable over long time periods. The large confidence intervals in the figure are notable. They are related to differences between taxels. However, the dispersion

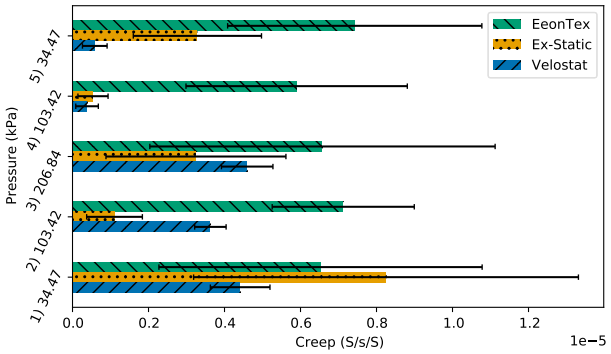

Fig. 7. Creep of the materials. The ordinal number before the parenthesis on the ordinate axis indicates the sequence of applied pressures. Bar errors indicate confidence intervals.

is clearly lower for Velostat. Those differences can be related to the inherent imperfections of manual manufacturing. Creep is more sensitive to them compared with other parameters.

Moreover, in this test Velostat has a different behavior when the material has been loaded previously with a higher pressure, as pointed out in [43] and [44], with a reduction in Creep of 65.23% with respect to the situation without previous load. This behavior is also noticeable in Ex-Static. In this regard, it would be important to control load history for better reproducibility in everyday use. This phenomenon is well known in these types of sensors, having been reported in other studies and by the manufacturers themselves [43], [45], [46], [47]. Therefore, preloading the sensor before use is highly recommended for better performance.

A window size of 30 s was selected for calculating the drift. According to our experimental results, the variations due to creep in such a window can be neglected when obtaining the drift, thus confirming the suitability of the selected window size.

C. Hysteresis

The hysteresis effect can be clearly seen in Fig. 8, in which Velostat seems to be less affected by hysteresis in comparison with Ex-Static and EeonTex. This point is also noticeable when the hysteresis is quantified, see Figs. 9 and 10.

However, it should be noted that the values of this parameter corresponding to the highest pressure loops of the ascendant tests are abnormally high (the cases corresponding to 165.47 and 193.05 kPa in Fig. 10). This is because they are associated with the smallest hysteresis loops near the saturation region in Fig. 8 (ascendant tests). Both the numerator and the denominator in (4) are small in those loops so that its ratio shows a high uncertainty. This problem would also appear with other hysteresis metrics because it is due to the almost flat behavior in the saturation region.

The data measured in the hysteresis tests can be used to obtain an estimation of the durability that some authors consider after applying many repetitions of periodic signals [14], [48]. For that purpose, the repetitions of the hysteresis cycles have been considered separately, instead of averaging them. Each repetition is different, which is also clearly shown by the variability parameter in fact. For instance, let us focus on the descendent hysteresis tests that were repeated ten times. Each

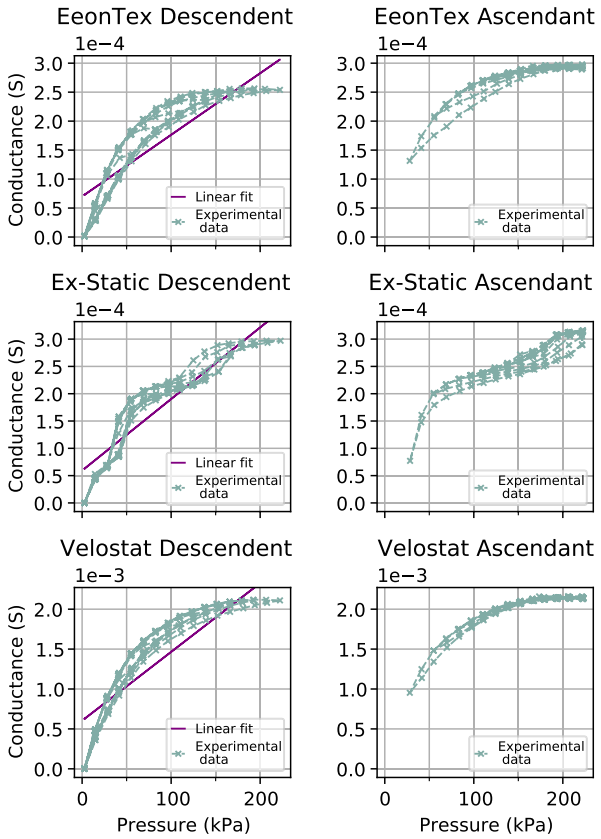

Fig. 8. Hysteresis response of a taxel for each material. The purple line is a linear fit.

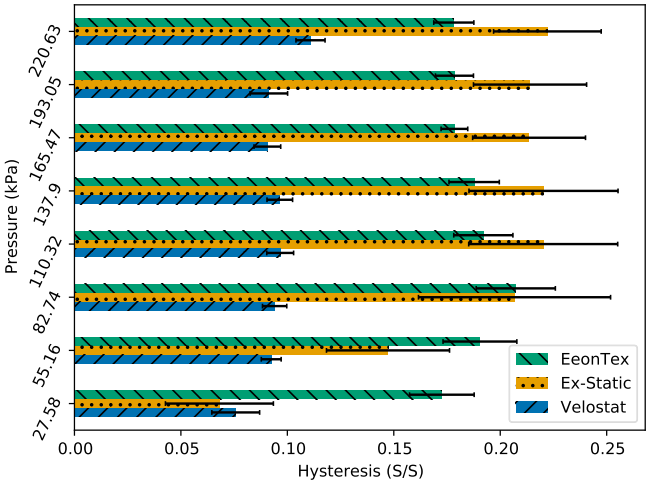

Fig. 9. Descendent hysteresis of the materials. Bar errors indicate confidence intervals.

repetition involved eight hysteresis cycles, although not all of them with the same pressure peak. Thus, a total of 80 cycles were applied. A quantitative measure of the change can be obtained by considering the difference in conductance at maximum pressure between the last and the second repetition on the largest hysteresis loop (first cycle in each repetition, 220.63-kPa peak value). The first repetition is excluded to account for preloading effects. Changes of 10%, 6%, and 7% have been obtained for Velostat, Ex-Static, and EeonTex, respectively.

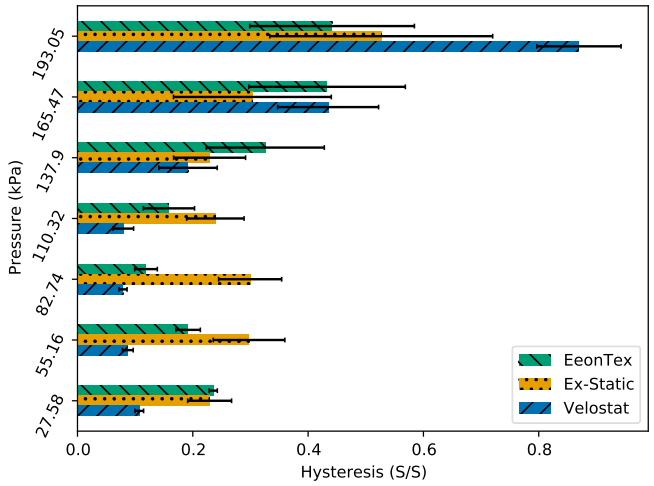

Fig. 10. Ascendant hysteresis of the materials. Bar errors indicate confidence intervals.

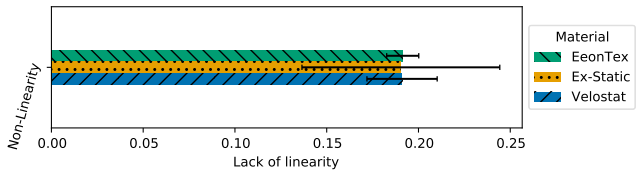

Fig. 11. Lack of linearity of the materials. Bar errors indicate confidence intervals.

D. Nonlinearity

The nonlinearity of the materials is significant, near 0.2, but it is similar in all of them. Fig. 11 presents the nonlinearity values. In Fig. 8, the linear fit of the descendent hysteresis curves can also be observed. The R^2 coefficients are 0.809, 0.810, and 0.809 for EeonTex, Ex-Static, and Velostat, respectively. A parameter that defines the sensitivity in piezoresistive sensors is the gauge factor, which has been defined and studied in different works [16], [49]. However, in this case the principle of operation of these sensors is the increase of the effective contact area between the piezoresistive material and the electrodes as the pressure applied increases [50], [51], [52]. Therefore, we could define the sensitivity as the slope of the linear fit, that is 1.14, 1.87, and 5.39 μS/kPa for EeonTex, Ex-Static, and Velostat, respectively. It can be seen that these sensitivities are consistent with those reported by other state-of-the-art studies [32], [33], which are sensors developed for different operation ranges and applications.

E. Response Time

Response time is presented in Fig. 12. Velostat is the fastest material (0.21 s), EeonTex is the slowest (0.50 s), while Ex-Static exhibits a delay of 0.42 s. The response to the pressure step function is also shown in Fig. 13 where the taxels have been averaged for the sake of clarity. It is also observed qualitatively that Velostat is the first to change.

F. Radar Chart Visualization

The radar chart in Fig. 14 allows the effects to be displayed together. Average values of the parameters are shown if

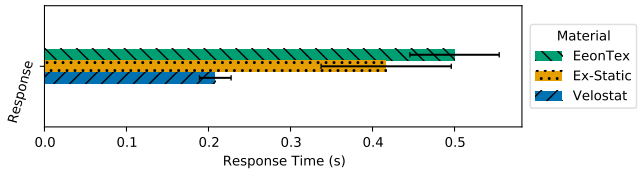

Fig. 12. Response time of the materials. Bar errors indicate confidence intervals.

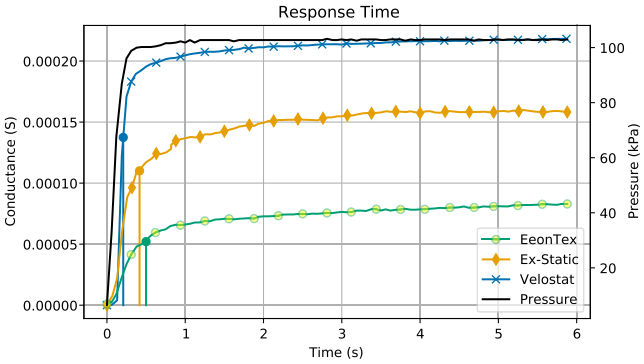

Fig. 13. Response to a step function. Three experiments are shown together (one for each material). For the sake of clarity, taxels are averaged for each material and pressure is averaged over the three experiments.

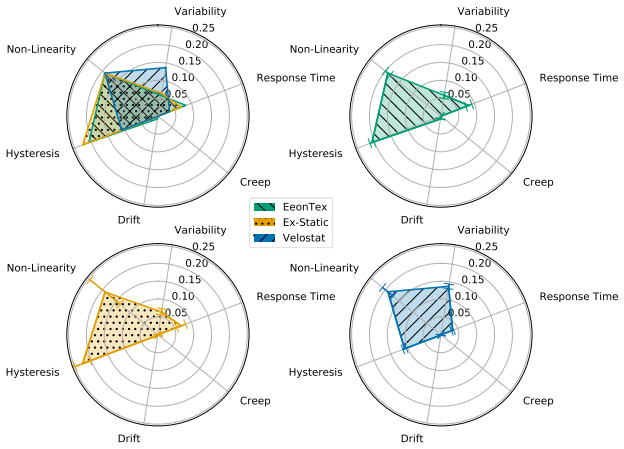

Fig. 14. Radar Chart of the nonidealities. Top left radar chart compares the three materials together, while the others show each material individually with bar errors indicating confidence intervals.

they have been calculated in Sections III-A–III-E for several pressure levels or conditions. Variability, drift, and hysteresis can be compared directly because they are relative values, whereas the creep value has been taken over 1-min period, which seems reasonable in this article because the stability tests lasted 30 s and there was an additional time while the volunteer stepped onto the platforms before starting the trials. Besides, the response time has been divided by 6 s, which is the end time used to calculate it.

The most important effects in this overview chart are hysteresis, nonlinearity, variability, and response time, while creep and drift have much lower numerical values. The lowest shaded area value in the chart corresponds to Velostat, which implies a better behavior, while the largest one corresponds to EeonTex, but very close to Ex-Static. It is worth mentioning

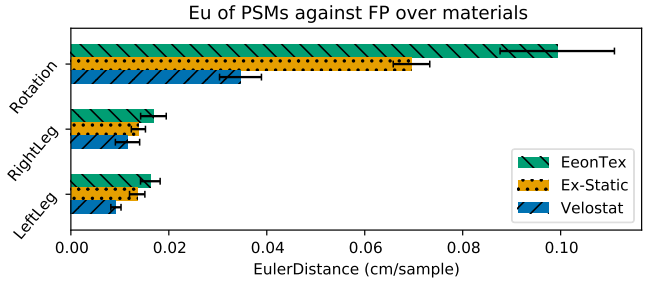

Fig. 15. Eu of the CoP trajectories by materials. Bar errors indicate confidence intervals.

that the differences that appear are unlikely to be due to changes in temperature because the temperature variations between experiments with different materials were small: less than 1 °C, except for the hysteresis experiment, in which they were less than 2.5 °C. For instance, the parameters of a Modified Prandt Ishlinskii model of hysteresis in another Velostat-based PSM [53] change less than 3.7% with a temperature difference of 2.5 °C, as can be deduced from data in [53].

IV. Results of the Stability Tests

The tests described in Section II-C were evaluated by comparing the CoP trajectories obtained by the FP (x_{FP}, y_{FP}) with those obtained by the PSMs (x_{PSM}, y_{PSM}). The figure of merit is the Euclidean distance between trajectories [54] divided by the number of points in the trajectory (N), referred to as Eu

$$\mathrm{Eu} = \frac{\sqrt{\sum_{i=1}^{N}\left(x_{\mathrm{PSM},i} - x_{\mathrm{FP},i}\right)^2 + \left(y_{\mathrm{PSM},i} - y_{\mathrm{FP},i}\right)^2}}{N}. \quad (6)$$

Fig. 15 shows the differences in CoP for each type of test after averaging over volunteers (confidence interval of the mean is also shown). Velostat is the material with the best performance in this regard, while EeonTex is the worst (Eu values averaged over all the experiments are 0.021, 0.035, and 0.045 cm/sample for Velostat, Ex-Static, and EeonTex, respectively). The differences are proportionally larger in the rotation experiment. In general, Eu depends on window size and sampling frequency. Future comparison with other studies should take this into account.

Once again, the differences are unlikely to be due to temperature changes. The three PSMs were tested just one after the other for a given volunteer. All in all, he/she did not stay more than 30 min, so there were no large temperature variations between the experiments with different materials. Besides, the order of PSMs was randomly selected for each volunteer.

A visual way to check the differences is to plot the trajectory coordinates directly. Two specific examples are shown in Figs. 16 (rotation) and 17 (single-legged). It is clearly observed that the Velostat-based PSM provides a trajectory closer to the reference instrument in the rotation experiment. The difference is not so clear in the single-legged trial, and the selection of the best PSM would depend on which part of the sequence one looks at. Anyway, the numerical values of Eu in Fig. 17

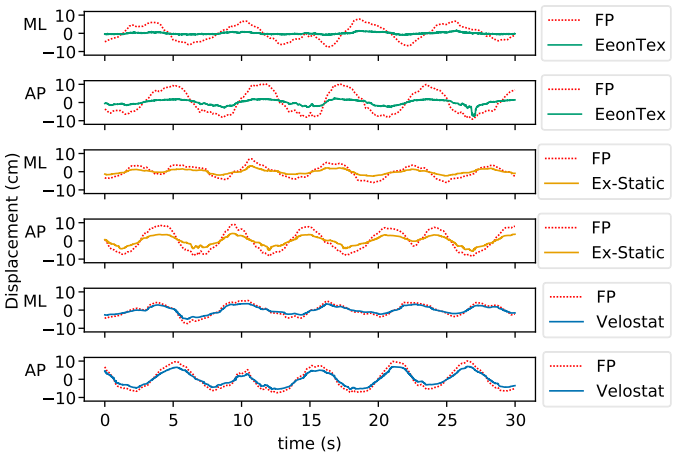

Fig. 16. CoP path of the rotation movement corresponding to the PSMs and FP in the ML and AP axes.

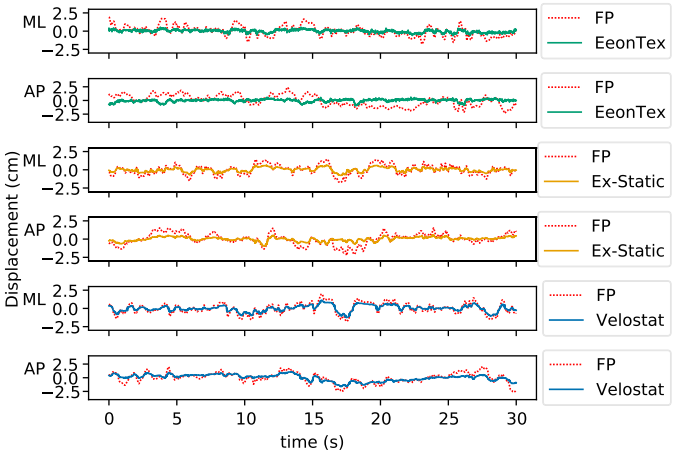

Fig. 17. CoP path of the single-legged movement corresponding to the PSMs and FP in the ML and AP axes.

are 0.011, 0.012, and 0.019 cm/sample for Velostat, Ex-Static, and EeonTex, respectively.

In an overall view of the results concerning the CoP trajectories and the effects analyzed in the sensor characterization, the best performance of the Velostat-based PSM can be explained both by its lower response time (at least two times better than the value of the other two materials) and by its hysteresis, which is lower than that of the other materials (the average hysteresis values are 0.11, 0.21, and 0.23 S/S for Velostat, EeonTex, and Ex-Static, respectively). Given that the hysteresis values of EeonTex and Ex-Static are similar, the difference in performances to measure CoP between them can be explained by their difference in response time (EeonTex is about 20% slower). Besides, that difference can also be due to a problem that we have noticed regarding the crosstalk elimination algorithm. This algorithm was initially tested with a Velostat-based PSM [34]. It has also been effective for the Ex-Static mat. On the other hand, we have noticed that the same numerical method does not remove ghost objects completely in the Eeon-Tex mat. This leads to a worse measurement of the CoP. It has been found that this happens even after adjusting the parameters of the algorithms to favor solution stability over speed or using a least-squares approach, which obtained the best results in [34]. The trouble of the numerical method in the EeonTex-based mat can be related to its high drift value, which indicates a random component in the output to which the algorithm is sensitive.

On the other hand, Velostat has a large variability (average value of 0.137 versus 0.065 and 0.059 S/S for Ex-Static and EeonTex, respectively), but this effect is not so relevant in the balance test. This might be due to the fact that the CoP is obtained from a weighted sum of taxels in the PSMs and in such situations even low-cost sensors are good enough to provide information about contact location [55]. For instance, in [55] it was found that variations due to mismatching between taxels were less relevant than hysteresis to measure the centroid of several objects.

Regarding creep, it has no influence on short trials. Besides, creep seems to decrease once a taxel has been loaded, which is clearly the case for many taxels in stability tests.

V. Conclusion

In this article, we have quantified several nonideal behaviors of three piezoresistive materials: Velostat, EeonTex, and Ex-Static. We have analyzed the influence on the sensor output of variability, creep, drift, hysteresis, nonlinearity, and response time.

It has been found that the material that shows less hysteresis is Velostat, while Ex-Static and EeonTex show less variability. It has been observed that the drift of Velostat and Ex-Static is lower. With respect to creep, it has been found that its value depends on the applied pressure. Besides, the Ex-Static creep and to a greater extent the Velostat creep, decrease when the material has been loaded previously. Finally, Velostat has the fastest response to sudden pressure changes.

We have also quantified the differences in the outcome of PSMs depending on the sensitive layer material in a specific application (the measurement of the CoP in balance tests with humans). The difference in their performances is compatible with a higher influence of response time and hysteresis in this kind of tests. Moreover, a correct crosstalk reduction is also relevant. Velostat is the most suitable material in this application. It is likely to be the most popular material to build low-cost tactile sensors. Our study helps to alleviate the lack of previous works that compare it with other alternatives and that allow a selection based on quantitative criteria.

This study presents two limitations. A fully dynamic sensor characterization as a function of frequency could not be carried out because the equipment does not allow applying sinusoidal loads with varying frequency (in the range 0.1–10 Hz for instance). Moreover, the crosstalk elimination algorithm did not remove it satisfactorily in one of the materials. It is likely that algorithms that require complex operations are more sensitive to noise. Using a better DAQ circuit that removes it without post-processing will be tested in the future, for instance, variants of zero potential or voltage feedback methods [56].

Further research could determine the quantification of the relationship between the nonideal behaviors analyzed in the

article and the CoP measurement. This would require the use of mathematical models for them. This relationship can be used to establish thresholds for the effects depending on the required performance or even compensate for them. Given that nonideal behavior depends on temperature and this might be relevant for some applications [57], it would be interesting to include temperature coefficients in the mathematical models so as to be able to compensate for them at different temperatures. Besides, it would be interesting to consider the long-term change of the material, like the study of Fatema et al. [58], but focusing on specific biomechanical applications like CoP measurement, and the effectiveness of these PSMs in clinical studies [59], [60].

Finally, being aware that a dynamic characterization could be relevant for some applications involving human movement, a complete dynamic study could be carried out with the appropriate characterization equipment.

REFERENCES

[1] G. Harman, "Pressure sensors," in *Sensor Technology Handbook*, J. S. Wilson, Ed., Burlington, NJ, USA: Newnes, Jan. 2005, ch. 1, pp. 411–456.

[2] S. Zhao, D. Liu, and F. Yan, "Wearable resistive-type stretchable strain sensors: Materials and applications," *Adv. Mater.*, vol. 37, no. 5, Feb. 2025, Art. no. 2413929.

[3] W. Fukui et al., "High-speed tactile sensing for array-type tactile sensor and object manipulation based on tactile information," *J. Robot.*, vol. 2011, Dec. 2011, Art. no. 691769.

[4] Y.-T. Chen et al., "Tongue pressure sensing array integrated with a system-on-chip embedded in a mandibular advancement splint," *Micromachines*, vol. 9, no. 7, p. 352, Jul. 2018.

[5] H. Liu, E. Sánchez, J. P. Parkerson, and A. Nelson, "Poster abstract: Unobtrusive sleep monitoring with low-cost pressure sensor array," in *Proc. IEEE/ACM Int. Conf. Connected Health, Appl.*, Sep. 2019, pp. 17–18.

[6] V. N. Quy et al., "Wearable device for monitoring heart rate based on low-cost piezoresistive sensor," in *Proc. 8th Int. Conf. Modern Circuits Syst. Technol. (MOCAST)*, May 2019, pp. 1–4.

[7] J. Hu, G. Dun, X. Geng, J. Chen, X. Wu, and T.-L. Ren, "Recent progress in flexible micro-pressure sensors for wearable health monitoring," *Nanosc. Adv.*, vol. 5, no. 12, pp. 3131–3145, 2023.

[8] J. Sánchez-Durán, F. Vidal-Verdú, Ó. Oballe-Peinado, J. Castellanos-Ramos, and J. Hidalgo-López, "A new model based on adaptation of the external loop to compensate the hysteresis of tactile sensors," *Sensors*, vol. 15, no. 10, pp. 26170–26197, Oct. 2015.

[9] H. Lee, H. Cho, S. J. Kim, Y. Kim, and J. Kim, "Dispenser printing of piezo-resistive nanocomposite on woven elastic fabric and hysteresis compensation for skin-mountable stretch sensing," *Smart Mater. Struct.*, vol. 27, no. 2, Jan. 2018, Art. no. 025017.

[10] A. Arndt, "Correction for sensor creep in the evaluation of long-term plantar pressure data," *J. Biomechanics*, vol. 36, no. 12, pp. 1813–1817, Dec. 2003.

[11] S. R. Chacko and S. M. Sivakumar, "A procedure for correction of creep in foam rubber optical pressure measurement techniques," *Experim. Mech.*, vol. 39, no. 2, pp. 125–131, Jun. 1999.

[12] H. S. Han, J. Yoon, S. Nam, S. Park, and D. J. Hyun, "A soft ground reaction force sensor system utilizing time-delay recurrent neural network," *IEEE Sensors J.*, vol. 20, no. 18, pp. 10851–10861, Sep. 2020.

[13] H. Park, J. Cho, J. Park, Y. Na, and J. Kim, "Sim-to-real transfer learning approach for tracking multi-DOF ankle motions using soft strain sensors," *IEEE Robot. Autom. Lett.*, vol. 5, no. 2, pp. 3525–3532, Apr. 2020.

[14] L. Lu, G. Hu, J. Liu, and B. Yang, "5G NB-IoT system integrated with high-performance fiber sensor inspired by cirrus and spider structures," *Adv. Sci.*, vol. 11, no. 18, May 2024, Art. no. 2309894.

[15] B. Taherkhani, A. Tuncay Atalay, and O. Atalay, "A comparative study on the multidirectional piezo-resistive scenario of conventional and auxetic silicone-based sensors coated with graphite powder," *Proc. Inst. Mech. Engineers, Part L: J. Materials: Design Appl.*, vol. 239, no. 1, pp. 90–99, Jan. 2025.

[16] D. D. L. Chung, "A critical review of piezoresistivity and its application in electrical-resistance-based strain sensing," *J. Mater. Sci.*, vol. 55, no. 32, pp. 15367–15396, Nov. 2020.

[17] C. Lebosse, P. Renaud, B. Bayle, and M. de Mathelin, "Modeling and evaluation of low-cost force sensors," *IEEE Trans. Robot.*, vol. 27, no. 4, pp. 815–822, Aug. 2011.

[18] A. Saxena and K. Patra, "Recent developments in stretchable and flexible tactile sensors towards piezoresistive systems: A review," *Polym. for Adv. Technol.*, vol. 35, no. 1, p. 6251, Jan. 2024.

[19] S. Nizami, M. Cohen-McFarlane, J. R. Green, and R. Goubran, "Comparing metrological properties of pressure-sensitive mats for continuous patient monitoring," in *Proc. IEEE Sensors Appl. Symp. (SAS)*, Mar. 2017, pp. 1–6.

[20] *Metrological Regulation for Load Cells*, Int. Recommendation, Organisation Internationale De Métrologie Légalen, Paris, Nov. 2000.

[21] J. Woodburn and P. Helliwell, "Observations on the F-scan in-shoe pressure measuring system," *Clin. Biomechanics*, vol. 11, no. 5, pp. 301–304, Jul. 1996.

[22] D. A. Valle-Lopera, A. F. Castraño-Franco, J. Gallego-Londoño, and A. M. Hernández-Valdivieso, "Test and fabrication of piezoresistive sensors for contact pressure measurement," *Revista Facultad de Ingeniería Universidad de Antioquia*, vol. 2017, no. 82, pp. 47–52, Mar. 2017.

[23] J. Deng, Y. Liu, J. Li, S. Zhang, and K. Li, "Displacement linearity improving method of stepping piezoelectric platform based on leg wagging mechanism," *IEEE Trans. Ind. Electron.*, vol. 69, no. 6, pp. 6429–6432, Jun. 2022.

[24] M. Y. Li, I. Galton, L. E. Larson, and P. M. Asbeck, "Correlation techniques for estimation of amplifier nonlinearity," in *Proc. IEEE Radio Wireless Conf.*, 2004, pp. 179–182.

[25] B. Ratner, "The correlation coefficient: Its values range between +1/- 1, or do they?" *J. Targeting*, vol. 17, no. 2, pp. 139–142, Jun. 2009.

[26] A. Brenton-Rule et al., "Reliability of the TekScan MatScan® system for the measurement of postural stability in older people with rheumatoid arthritis," *J. Foot Ankle Res.*, vol. 5, no. 1, pp. 1–7, Jan. 2012.

[27] A. Desai, V. Goodman, N. Kapadia, B. L. Shay, and T. Szturm, "Relationship between dynamic balance measures and functional performance in community-dwelling elderly people," *Phys. Therapy*, vol. 90, no. 5, pp. 748–760, May 2010.

[28] A. E. Chisholm, S. D. Perry, and W. E. McIlroy, "Inter-limb centre of pressure symmetry during gait among stroke survivors," *Gait Posture*, vol. 33, no. 2, pp. 238–243, Feb. 2011.

[29] A. D. Bincalar, C. Freeman, and M. C. Schraefel, "Optimal algorithms for improving pressure-sensitive mat centre of pressure measurements," *Sensors*, vol. 25, no. 5, p. 1283, Feb. 2025.

[30] J. Martínez-Cesteros, "Development of a low cost pressure sensitive mat: Application to stability and posture measurement," Ph.D. dissertation, Doctoral Program Electron. Eng., Dept. Electron. Eng. Commun., University of Zaragoza, Zaragoza, Spain, 2023.

[31] R. Barba, Á. P. de Madrid, and J. G. Boticario, "Development of an inexpensive sensor network for recognition of sitting posture," *Int. J. Distrib. Sensor Netw.*, vol. 11, no. 8, Aug. 2015, Art. no. 969237.

[32] A. Dzedzickis et al., "Polyethylene-carbon composite (Velostat®) based tactile sensor," *Polymers*, vol. 12, no. 12, p. 2905, Dec. 2020.

[33] A. G. Ferreira, A. P. Catarino, J. L. Monteiro, and A. M. Rocha, "Textile-based pressure sensors for step detection: A preliminary assessment," *IOP Conf. Ser., Mater. Sci. Eng.*, vol. 459, Dec. 2018, Art. no. 012041.

[34] C. Medrano-Sánchez, R. Igual-Catalán, V. H. Rodríguez-Ontiveros, and I. Plaza-García, "Circuit analysis of matrix-like resistor networks for eliminating crosstalk in pressure sensitive mats," *IEEE Sensors J.*, vol. 19, no. 18, pp. 8027–8036, Sep. 2019.

[35] J. Martinez-Cesteros, C. Medrano-Sanchez, I. Plaza-Garcia, R. Igual-Catalan, and S. Albiol-Pérez, "A velostat-based pressure-sensitive mat for center-of-pressure measurements: A preliminary study," *Int. J. Environ. Res. Public Health*, vol. 18, no. 11, p. 5958, Jun. 2021.

[36] *Pb100e Equilibration Device. Tekscan*. Accessed: Jan. 25, 2023. [Online]. Available: https://www.tekscan.com/products-solutions/equilibrators/pb100e-equilibration-device

[37] *Pneumax Regulador De Presión Proporcional*. Accessed: Jan. 25, 2023. [Online]. Available: https://pneumaxspa.com/en/product-news/regolatori-proporzionali-serie-1700-versione-ethercat/

[38] D. Z. Morgado Ramirez, M. del Pilar Garcia Souto, B. M. Oldfrey, P. Smitham, M. Miodownik, and C. Holloway, "Characterization of bespoke force sensors for tailored applications," *IEEE Sensors J.*, vol. 17, no. 6, pp. 1727–1734, Mar. 2017.

[39] M. Hamilton, K. Behdinan, and J. Andrysek, "Evaluating the effects of load area and sensor configuration on the performance of pressure sensors at simulated body-device interfaces," *IEEE Sensors J.*, vol. 20, no. 10, pp. 5187–5194, May 2020.

[40] C. Lin, S. Zheng, P. Li, Z. Shen, and S. Wang, "Positioning error analysis and control of a piezo-driven 6-DOF micro-positioner," *Micromachines*, vol. 10, no. 8, p. 542, Aug. 2019.

[41] *Official Website of Pasco*. Accessed: Dec. 30, 2022. [Online]. Available: https://www.pasco.com/products/sensors/force/ps-2141

[42] J. Martínez-Cesteros, C. Medrano-Sánchez, J. Castellanos-Ramos, J. A. Sánchez-Durán, and I. Plaza-García, "Creep and hysteresis compensation in pressure-sensitive mats for improving center-of-pressure measurements," *IEEE Sensors J.*, vol. 23, no. 23, pp. 29585–29593, Dec. 2023.

[43] Z. Wang, Y. Dong, H. Zhu, and G. Feng, "Creep characteristics of combined bulk acoustic wave quartz resonator force sensors," *Sens. Actuators A, Phys.*, vol. 111, nos. 2–3, pp. 203–209, Mar. 2004.

[44] A. Hollinger and M. Wanderley, "Evaluation of commercial force-sensing resistors," in *Proc. New Interfaces Musical Expression, NIME06*, Paris, Jun. 2006, pp. 4–8.

[45] *Tekscan. FAQ: Why do You Need to Condition a Flexiforce® Sensor?* Accessed: Aug. 31, 2025. [Online]. Available: https://www.tekscan.com/support/faqs/why-do-you-need-condition-flexiforce-sensor

[46] *Tekscan. Calibration Quick Start Guide for Flexiforce™ Sensors*. Accessed: Sep. 1, 2025. [Online]. Available: https://www.tekscan.com/products-solutions/equilibrators/pb100e-equilibration-device

[47] J. M. Brimacombe, D. R. Wilson, A. J. Hodgson, K. C. T. Ho, and C. Anglin, "Effect of calibration method on tekscan sensor accuracy," *J. Biomechanical Eng.*, vol. 131, no. 3, Mar. 2009, Art. no. 034503.

[48] K. Qin et al., "Magnetic array assisted triboelectric nanogenerator sensor for real-time gesture interaction," *Nano-Micro Lett.*, vol. 13, no. 51, pp. 1–9, 2021.

[49] V. Belwanshi, "Analytical modeling to estimate the sensitivity of MEMS technology-based piezoresistive pressure sensor," *J. Comput. Electron.*, vol. 20, no. 1, pp. 668–680, Feb. 2021.

[50] J. Castellanos-Ramos, R. Navas-González, I. Fernández, and F. Vidal-Verdú, "Insights into the mechanical behaviour of a layered flexible tactile sensor," *Sensors*, vol. 15, no. 10, pp. 25433–25462, Oct. 2015.

[51] J. A. Greenwood, "Constriction resistance and the real area of contact," *Brit. J. Appl. Phys.*, vol. 17, no. 12, pp. 1621–1632, Dec. 1966.

[52] J. R. Barber, "Incremental stiffness and electrical contact conductance in the contact of rough finite bodies," *Phys. Rev. E, Stat. Phys. Plasmas Fluids Relat. Interdiscip. Top.*, vol. 87, no. 1, Jan. 2013, Art. no. 013203.

[53] S. Domínguez-Gimeno, C. Medrano-Sanchez, R. Igual-Catalan, and I. Plaza-Garcia, "Optimized creep-hysteresis model to improve center-of-pressure detection in pressure-sensitive mats," *IEEE Sensors J.*, vol. 25, no. 9, pp. 15295–15306, May 2025.

[54] Y. Tao et al., "A comparative analysis of trajectory similarity measures," *GIScience Remote Sens.*, vol. 58, no. 5, pp. 643–669, Jul. 2021.

[55] J. Sánchez-Durán, J. Hidalgo-López, J. Castellanos-Ramos, Ó. Oballe-Peinado, and F. Vidal-Verdú, "Influence of errors in tactile sensors on some high level parameters used for manipulation with robotic hands," *Sensors*, vol. 15, no. 8, pp. 20409–20435, Aug. 2015.

[56] J.-F. Wu, "Scanning approaches of 2-D resistive sensor arrays: A review," *IEEE Sensors J.*, vol. 17, no. 4, pp. 914–925, Feb. 2017.

[57] V. Belwanshi, S. Philip, and A. Topkar, "Performance study of MEMS piezoresistive pressure sensors at elevated temperatures," *IEEE Sensors J.*, vol. 22, no. 10, pp. 9313–9320, May 2022.

[58] A. Fatema, S. Chauhan, M. D. Gupta, and A. M. Hussain, "Investigation of the long-term reliability of a velostat-based flexible pressure sensor array for 210 days," *IEEE Trans. Device Mater. Rel.*, vol. 24, no. 1, pp. 41–48, Mar. 2024.

[59] T. E. Prieto, J. B. Myklebust, R. G. Hoffmann, E. G. Lovett, and B. M. Myklebust, "Measures of postural steadiness: Differences between healthy young and elderly adults," *IEEE Trans. Biomed. Eng.*, vol. 43, no. 9, pp. 956–966, Sep. 1996.

[60] F. Quijoux et al., "Center of pressure displacement characteristics differentiate fall risk in older people: A systematic review with meta-analysis," *Ageing Res. Rev.*, vol. 62, Sep. 2020, Art. no. 101117.